Engineering of Efficient Panchromatic Sensitizers for Nanocrystalline TiO_2-Based Solar Cells

Mohammad K. Nazeeruddin,* Peter Péchy, Thierry Renouard, Shaik M. Zakeeruddin, Robin Humphry-Baker, Pascal Comte, Paul Liska, Le Cevey, Emiliana Costa,† Valery Shklover,‡ Leone Spiccia,§ Glen B. Deacon,§ Carlo A. Bignozzi,† and Michael Grätzel*

Contribution from the Laboratory for Photonics and Interfaces, Institute of Physical Chemistry, Swiss Federal Institute of Technology, CH-1015 Lausanne, Switzerland

Received September 7, 2000

Abstract: A new series of panchromatic ruthenium(II) sensitizers derived from carboxylated terpyridyl complexes of tris-thiocyanato Ru(II) have been developed. Black dye containing different degrees of protonation $\{(C_2H_5)_3NH\}[Ru(H_3tcterpy)(NCS)_3]$ **1**, $\{(C_4H_9)_4N\}_2[Ru(H_2tcterpy)(NCS)_3]$ **2**, $\{(C_4H_9)_4N\}_3[Ru(Htcterpy)(NCS)_3]$ **3**, and $\{(C_4H_9)_4N\}_4[Ru(tcterpy)(NCS)_3]$ **4** (tcterpy = 4,4′,4″-tricarboxy-2,2′:6′,2″-terpyridine) have been synthesized and fully characterized by UV−vis, emission, IR, Raman, NMR, cyclic voltammetry, and X-ray diffraction studies. The crystal structure of complex **2** confirms the presence of a $Ru^{II}N6$ central core derived from the terpyridine ligand and three N-bonded thiocyanates. Intermolecular H-bonding between carboxylates on neighboring terpyridines gives rise to 2-D H-bonded arrays. The absorption and emission maxima of the black dye show a bathochromic shift with decreasing pH and exhibit pH-dependent excited-state lifetimes. The red-shift of the emission maxima is due to better π-acceptor properties of the acid form that lowers the energy of the CT excited state. The low-energy metal-to-ligand charge-transfer absorption band showed marked solvatochromism due to the presence of thiocyanate ligands. The Ru(II)/(III) oxidation potential of the black dye and the ligand-based reduction potential shifted cathodically with decreasing number of protons and showed more reversible character. The adsorption of complex **3** from methoxyacetonitrile solution onto transparent TiO_2 films was interpreted by a Langmuir isotherm yielding an adsorption equilibrium constant, K_{ads}, of $(1.0 \pm 0.3) \times 10^5\ M^{-1}$. The amount of dye adsorbed at monolayer saturation was $(n_\alpha = 6.9 \pm 0.3) \times 10^{-8}$ mol/mg of TiO_2, which is around 30% less than that of the *cis*-di(thiocyanato)bis(2,2′-bipyridyl-4,4′-dicarboxylate)-ruthenium(II) complex. The black dye, when anchored to nanocrystalline TiO_2 films achieves very efficient sensitization over the whole visible range extending into the near-IR region up to 920 nm, yielding over 80% incident photon-to-current efficiencies (IPCE). Solar cells containing the black dye were subjected to analysis by a photovoltaic calibration laboratory (NREL, U.S.A.) to determine their solar-to-electric conversion efficiency under standard AM 1.5 sunlight. A short circuit photocurrent density obtained was 20.5 mA/cm^2, and the open circuit voltage was 0.72 V corresponding to an overall conversion efficiency of 10.4%.

1. Introduction

Dye-sensitized solar cell technology is an interesting and promising inexpensive alternative to the proven solid-state photovoltaic cells.[1] In recent years, many groups have been focusing their attention on fundamental aspects of dye-sensitized solar cell components.[2−9] Dye-derivatized mesoporous titania film is one of the key components in such cells. The electrochemical, photophysical, and ground- and excited-state properties of the dye play an important role for charge-transfer

* Author for correspondence. E-mail: Mdkhaja.Nazeeruddin@epfl.ch.
† Dipartimento de Chimica, Università di Ferrara, 44100 Ferrara, Italy.
‡ Laboratory of Crystallography, Swiss Federal Institute of Technology, 8092 Zurich, Switzerland.
§ Centre for Green Chemistry and Department of Chemistry, Monash University, Clayton, Vic. 3168, Australia.

(1) McConnell, R. D. Ed. *Future Generation Photovoltaic Technologies*; American Institute of Physics Conference Proceedings 404, Denver, 1997.
(2) (a) Schlichthörl, G.; Park, N. G.; Frank, A. J. *J. Phys. Chem. B* **1999**, *103*, 782. (b) Huang, S. Y.; Schlichthörl, G.; Nozik, A. J.; Grätzel, M.; Frank, A. J. *J. Phys. Chem. B* **1997**, *101*, 2576. (c) Schlichthörl, G.; Huang, S. Y.; Frank, A. J. *J. Phys. Chem. B* **1997**, *101*, 8141.
(3) (a) Zaban, A.; Ferrrere, S.; Sprague, J.; Gregg, B. A. *J. Phys. Chem. B* **1997**, *101*, 55. (b) Ferrrere, S.; Gregg, B. A. *J. Am. Chem. Soc.* **1998**, *120*, 843. (c) Lemon, B. I.; Hupp, J. T. *J. Phys. Chem. B* **1999**, *103*, 3797. (d) Langdon, B. T.; MacKenzie, V. J.; Asunskis, D. J.; Kelly, D. F. *J. Phys. Chem. B* **1999**, *103*, 11176.
(4) (a) Kelly, C. A.; Farzad, F.; Thompson, D. W.; Stipkala, J. M.; Meyer, G. J. *Langmuir* **1999**, *15*, 7047. (b) Thompson, D. W.; Kelly, C. A.; Farzad, F.; Meyer, G. J. *Langmuir* **1999**, *15*, 650.
(5) (a) Schwarzburg, K.; Willig, F. *J. Phys. Chem. B* **1999**, *103*, 5743. (b) Franco, G.; Gehring, J.; Peter, L. M.; Ponomarev, E. A.; Uhlendorf, I. *J. Phys. Chem. B* **1999**, *103*, 692. (c) Salafsky, J. S.; Lubberhuizen, W. H.; van Faassen, E.; Schropp, R. E. I. *J. Phys. Chem. B* **1998**, *102*, 766.
(6) Solbrand, A.; Henningsson, A.; Södergren, S.; Lindström, H.; Hagfeldt, A.; Lindquist, S.-E. *J. Phys. Chem. B* **1999**, *103*, 1078.
(7) (a) Bando, K. K.; Mitsuzuka, Y.; Sugino, M.; Sughihara, H.; Sayama, K.; Arakawa, H. *Chem. Lett.* **1999**, 853. (b) Sughihara, H.; Sing, L. P.; Sayama, K.; Arakawa, H.; Nazeeruddin, Md. K.; Grätzel, M. *Chem. Lett.* **1998**, 1005. (c) Sayama, K.; Sughihara, H.; Arakawa, H. *Chem. Mater.* **1998**, *10*, 3825. (d) Murakoshi, K.; Kano, G.; Wada, Y.; Yanagida, S.; Miyazaki, H.; Matsumoto, M.; Murasawa, S. *J. Electroanal. Chem.* **1995**, *396*, 27.
(8) (a) Argazzi, R.; Bignozzi, C. A.; Heimer, T. A.; Meyer, G. J. *Inorg. Chem.* **1997**, *36*, 2. (b) Argazzi, R.; Bignozzi, C. A.; Hasselmann, G. M.; Meyer, G. J. *Inorg. Chem.* **1998**, *37*, 4533.
(9) (a) Tennakone, K.; Kumara, G. R. R. A.; Kottegoda, I. R. M.; Perera, V. P. S. *Chem. Commun.* **1999**, 15. (b) Nasr, C.; Hotchandani, S.; Kamat, P. V. *J. Phys. Chem. B* **1998**, *102*, 4944−4951. (c) Ihara, M.; Tanaka, K.; Sakaki, K.; Honma, I.; Yamada, K. *J. Phys. Chem. B* **1997**, *101*, 5153. (d) Jing, B.; Zhang, H.; Zhang, M.; Lu, Z.; Shen, T. *J. Mater. Chem.* **1998**, *8*, 2055.

10.1021/ja003299u CCC: $20.00
Published on Web 02/03/2001

dynamics at the semiconductor interface.[10] The electron injection rates have been measured in different laboratories using the *cis*-di(thiocyanato)bis(2,2′-bipyridyl-4,4′-dicarboxylate) ruthenium(II) complex (referred as N3) and were found to occur in the femtosecond time scale.[11] We and others have obtained incident photon-to-current conversion efficiencies (IPCE) of 80−85%, using N3 as a charge-transfer sensitizer.[12] However, the main drawback of this sensitizer is the lack of absorption in the red region of the visible spectrum.

The optimal sensitizer for the dye-sensitized solar cell should be panchromatic, that is, absorb visible light of all colors. Ideally, all photons below a threshold wavelength of about 920 nm should be harvested and converted to electric current. This limit is derived from thermodynamic considerations showing that the conversion efficiency of any single-junction photovoltaic solar converter peaks at approximately 33% near a threshold energy of 1.4 eV.[13] In addition, the sensitizer should fulfill several demanding conditions: (i) it must be firmly grafted to the semiconductor oxide surface and inject electrons into the conduction band with a quantum yield of unity, (ii) its redox potential should be sufficiently high so that it can be regenerated rapidly via electron donation from the electrolyte or a hole conductor, (iii) it should be stable enough to sustain at least 10^8 redox turnovers under illumination corresponding to about 20 years of exposure to natural sunlight.

Molecular engineering of ruthenium complexes that can act as panchromatic charge-transfer sensitizers for TiO_2-based solar cells presents a challenging task as several requirements have to be fulfilled by the dye which are very difficult to be met simultaneously. The LUMO and HOMO have to be maintained at levels where photoinduced electron transfer in the TiO_2 conduction band and regeneration of the dye by iodide can take place at practically 100% yield. This restricts greatly the options available to accomplish the desired red-shift of the metal-to-ligand charge-transfer transitions (MLCT) to about 900 nm.

The spectral and redox properties of ruthenium polypyridyl complexes can be tuned in two ways. First, by introducing a ligand with a low-lying π^* molecular orbital and second by destabilization of the metal t_{2g} orbital through the introduction of a strong donor ligand. Meyer et al. have used these strategies to tune considerably the MLCT transitions in ruthenium complexes.[14] Heteroleptic complexes containing bidentate ligands with low-lying π^* orbitals together with others having strong σ-donating properties show indeed impressive panchromatic absorption properties.[14] However, the extension of the spectral response into the near-IR was gained at the expense of shifting the LUMO orbital to lower levels from where charge injection into the TiO_2 conduction band can no longer occur.[15]

Near-infrared response can also be gained by upward shifting of the Ru t_{2g} (HOMO) levels. However, it turns out that the mere introduction of strong sigma donor ligands into the complex often does not lead to the desired spectral result as both the HOMO and LUMO are displaced in the same direction. Furthermore, the HOMO position cannot be varied freely as the redox potential of the dye must be maintained sufficiently positive to ascertain rapid regeneration of the dye by electron donation from iodide following charge injection into the TiO_2.

In an effort to fulfill all of these demanding requirements of the sensitizer, we have engineered at the molecular level and synthesized a ruthenium(II) black dye in which the ruthenium center is coordinated to a monoprotonated tricarboxyterpyridine ligand (tcterpy = 4,4′,4″-tricarboxy-2,2′:6,2″-terpyridine) and three thiocyanate ligands. The purpose of incorporating carboxylate groups in the ligand is three-fold: (i) to increase the molar extinction coefficient of the complex, (ii) to facilitate the grafting of the dye on the semiconductor surface, and (iii) to ensure intimate electronic coupling between its excited-state wave function and the conduction band manifold of the semiconductor. It is well-known that substitution of carboxy groups at the 4,4′-positions of 2,2′-bipyridine affords an increase in the molar extinction coefficient of 40%.[16] The role of the thiocyanato ligands is to tune the metal t_{2g} orbitals of ruthenium(II) and possibly to stabilize the hole that is being generated on the metal, after having injected an electron into the conduction band. The reason for using the monoprotonated tcterpy was to diminish the formation of intermolecular hydrogen-bonded sheets. This reduces the aggregation of the dye on the TiO_2 surface.[17]

The black dye meets most of the requirements of an efficient sensitizer and exhibits better near-IR photoresponse than the N3 dye. Indeed, it shows the 920 nm absorption threshold which is ideal for a single-junction converter. This paper reports an improved synthesis of the 4,4′,4″-trimethoxycarbonyl-2,2′:6′,2″-terpyridine ligand and the black dye containing different degrees of protonation of the tcterpy ligand. A preliminary account of this work has been published elsewhere.[18]

2. Experimental Section

2.1. Materials. The solvents (puriss grade), potassium thiocyanate, ammonium thiocyanate, tetrabutylammonium thiocyanate, tetrabutylammonium hydroxide, 4-ethylpyridine, 10% Pd on activated carbon, and acidic-type Al_2O_3 for chromatography were purchased from Fluka. Hydrated ruthenium trichloride was purchased from Johnson Matthey and used as received. Sephadex LH-20 (Pharmacia) was allowed to swell in water for a minimum of 2 h before use.

2.2. Analytical Measurements. UV−vis and fluorescence spectra were recorded in a 1 cm path length quartz cell on a Cary 5 spectrophotometer and a Spex Fluorolog 112 spectrofluorometer, respectively. The emitted light was detected with a Hamamatsu R2658 photomultiplier operated in single-photon counting mode. The emission spectra were photometrically corrected using a calibrated 200 W tungsten lamp as reference source. The solutions were prepared to give approximate concentrations of 10 μM. The emission lifetimes were

(10) (a) Nazeeruddin, Md. K.; Muller, E.; Humphry-Baker, R.; Vlachopoulos, N.; Grätzel, M. *J. Chem. Soc., Dalton Trans.* **1997**, 4571. (b) Nazeeruddin, Md. K.; Zakeeruddin, S. M.; Humphry-Baker, R.; Jirousek, M.; Liska, P.; Vlachopoulos, N.; Shklover, V.; Fischer, C. H.; Grätzel, M. *Inorg. Chem.* **1999**, *38*, 6298.

(11) (a) Asbury, J. B.; Ellingson, R. J.; Ghosh, H. N.; Ferrere, S.; Nozik, A. J.; Lian, T. *J. Phys. Chem. B* **1999**, *103*, 3110. (b) Moser, J. E.; Noukakis, D.; Bach, U.; Tachibana, Y.; Klug, D. R.; Durrant, J. R.; Humphry-Baker, R.; Grätzel, M. *J. Phys. Chem. B* **1998**, *102*, 3649. (c). Haque, S. A.; Tachibana, Y.; Klug, D. R.; Durrant, J. R. *J. Phys. Chem. B* **1998**, *102*, 1745.

(12) (a) Nazeeruddin, Md. K.; Kay, A.; Rodicio, I.; Humphry-Baker, R.; Muller, E.; Liska, P.; Vlachopoulos, N.; Grätzel, M. *J. Am. Chem. Soc.* **1993**, *115*, 6382. (b) Hou, Y.-J.; Xie, P.-H.; Z. Jing, B.-W.; Cao, Y.; Xiao, X.-R.; Wang, W.-B. *Inorg. Chem.* **1999**, *38*, 6320.

(13) (a) Haught, A. F. *J. Solar Energy Eng.* **1984**, *106*, 3. (b) Winter, C.; Sizman, R.; Vant Hull, L. *Solar Power Plants*; Springer-Verlag: New York, 1991; Chapter 2. (c) De Vos, A. *Endoreversible Thermodynamics of Solar Energy Conversion*; Oxford Science Publishers: Oxford, 1992; Chapter 6. (d) Luque, A.; Araujo, G. *Physical Limitations to Photovoltaic Conversion*; Adam Hilger: New York, 1990; pp 106−134. (e) Baruch, P. *J. Appl. Phys*. **1985**, *57*, 1347.

(14) P. A. Anderson, P. A.; Strouse, G. F.; Treadway, J. A.; Keene F. R.; Meyer, T. J. *Inorg. Chem.* **1994**, *33*, 3863.

(15) (a) Treadway, J. A.; Moss, J. A.; Meyer, T. J. *Inorg. Chem*. **1999**, *38*, 4386. (b) Alebbi, M.; Bignozzi, C. A.; Heimer, T. A.; Hasselmann, G. M.; Meyer, G. J. *J. Phys. Chem. B* **1998**, *102*, 7577.

(16) Nazeeruddin, Md. K.; Kalyanasundaram, K.; Grätzel, M. *Inorg. Synth*. **1998**, *32*, 181.

(17) Zakeeruddin, S. M.; Nazeeruddin, Md. K.; Humphry-Baker, R.; Grätzel, M.; Shklover, V. *Inorg. Chem*. **1998**, *37*, 5251.

(18) Nazeeruddin, Md. K.; Pechy, P.; Grätzel, M. *Chem. Commun*. **1997**, 1705.

Table 1. Experimental Details of X-ray Structure Study for the Complex **2**

formula weight	1201.94 ($C_{55}H_{88}N_8O_7S_4Ru$)
crystal color, habit	dark brown, plate
crystal dimensions (mm)	0.2 × 0.15 × 0.03
crystal system	monoclinic
space group	*Cc*
lattice parameters	
a (Å)	32.1406(2)
b (Å)	23.2569(5)
c (Å)	23.3653(4)
β (deg)	133.062(1)
V (Å)	12760.90
Z	8
density calc (g cm^{-3})	1.258
absorption coefficient μK_α (mm^{-1})	9.39
F(000)	4896.0
T (K)	243
reflections measured	39594
independent reflections	19642
observed reflections	12471
used in refinement	7602
no. of refined parameters	751
residuals *R*, R_w	0.0873, 0.0754
reflections/parameters ratio	10.1
goodness of fit	7.198

measured by exciting the sample with a pulse from an active modelocked Nd:YAG laser, using the frequency doubled line at 532 nm. The emission decay was followed on a Tektronix DSA 640 digitizing signal analyzer, using a Hamamatsu R928 photomultiplier to convert the light signal to a voltage waveform.

Electrochemical data were obtained by cyclic voltammetry using a three-electrode cell and a BAS100 electrochemical analyzer. The working electrode was a 0.07 cm^2 glassy carbon disk, the auxiliary electrode was a glassy carbon rod, the reference electrode was AgCl/Ag, saturated KCl (0.197V vs SHE), and the supporting electrolyte was 0.1 M tetrabutylammonium tetrafluoroborate (TBATFB).

^{1}H NMR spectra were measured with Bruker ACP-200 or AMX2−600 spectrometers at 200 and 600 MHz, respectively. ^{13}C NMR spectra were measured with a Bruker ACP-200 at 50.3 MHz. The reported chemical shifts were against TMS.

Infrared spectra were obtained with a Perkin-Elmer Paragon 1000 FTIR spectrophotometer at a resolution of 5 cm^{-1} with the samples dispersed in compressed KBr pellets.

HPLC analysis was carried out on a Waters 600 equipped with PDA, using IC-Pak anion HR column. The eluent is aqueous 0.08 M $LiClO_4$ solution containing 2.5% acetonitrile.

Resonance Raman (RR) spectra were obtained on a 1877 Spex Triplemate spectrograph equipped with a Princeton Instruments liquid N_2 cooled CCD-1024E detector. A 1200 groove/mm grating was used giving a resolution of 2.5 cm^{-1}. Data acquisition was controlled by an Apple Power PC computer running Wavemetrics software to control the PI ST-135 controller and the Spex DM 3000 controller. All of the data were corrected for the spectral response of the instrument using a National Bureau of Standards light standard. INNOVA 200K Kr+ laser provided the excitation source. Aqueous solutions of typically 0.5 mM concentration were examined in 1 mm inner diameter capillaries, using a 90° scattering geometry.

2.3. X-ray Structure Determination. Single crystals of complex **2** were obtained from DMSO. When the solvent was allowed to evaporate slowly, the complex, $\{(C_4H_9)_4N\}_2[Ru(H_2tcterpy)(NCS)_3]$ **2** deposited as small crystals onto the walls of the flask. The data collection for a single crystal **2** was performed at 243 K on a Siemens SMART PLATFORM with CCD detector, using Mo Kα radiation, graphite monochromator, and *ω*-scan technique with an exposure time of 120 s/frame. Other experimental details and results of the structure refinement are depicted in Table 1. The H atoms were not localized, but in terpyridyl moieties they were placed in calculated positions and refined as "riding" atoms with fixed C−H distances and isotropic temperature factors $U = 0.08$ Å^{-2}. The O and C atoms of the solvate molecules (DMSO) were refined isotropically. The SHELXTL PLUS suite of programs was used for data reduction, structure solution, and refinement.[19]

2.4. Acid−Base Equilibria. Since the fully protonated black dye is insoluble in water, 16% of ethanol was added to avoid precipitation. A stock solution (5×10^{-5} M) was prepared in 100 cm^3 of 5.25/1 H_2O/ethanol mixture containing 0.1 M $NaNO_3$. The initial pH of the solution was adjusted to 11 by adding 0.2 M NaOH solution. (Note that the aqueous pH scale may no longer be meaningful once ethanol is added. However, at the concentration employed, ethanol had only a small effect on the pH reading of the glass electrode used.) The pH of the solution was lowered by the addition of 0.2 M HNO_3 solution. The UV−vis spectrum of each solution was measured after each addition of acid, after equilibration of the solution for 5 min. The emission spectra and the lifetime data were collected without degassing the solutions at room temperature by exciting into the lowest-energy MLCT band.

2.5. Photoelectrochemical Measurements. Photoelectrochemical data were measured using a 450 W xenon light source that was focused to give 1000 W/m^2, the equivalent of one sun at AM1.5, at the surface of the test cell. The spectral output of the lamp was matched in the region of 350−750 nm with the aid of a Schott KG-5 sunlight filter so as to reduce the mismatch between the simulated and the true Solar spectrum to less than 2%. The differing intensities were regulated with neutral wire mesh attenuators. The applied potential and measured cell current was measured using a Keithley model 2400 digital source meter. The current−voltage characteristics of the cell under these conditions were determined by biasing the cell externally and measuring the generated photocurrent. This process was fully automated using Wavemetrics software.[20] A similar data acquisition system was used to control the incident photon-to-current conversion efficiency (IPCE) measurement. Under full computer control, light from a 300 W Xe lamp was focused through a high throughput monochromator onto the photovoltaic cell under test. The monochromator was incremented through the visible spectrum to generate the IPCE (λ) curve as defined below,

$$\text{IPCE}\ (\lambda) = 1240\ (I_{sc}/\lambda\phi)$$

where λ is the wavelength, I_{sc} is the current at short circuit (mA/cm^2), and ϕ is the incident radiative flux (W/m^2). This curve can be derived from the measured absorption spectrum of the adsorbed photosensitizer for comparison.

2.6. TiO_2 Electrode Preparation. The acidic and basic TiO_2 colloids are prepared using published procedures.[21] The two colloids (acidic colloid 60% W/W TiO_2 and basic colloid 40% W/W TiO_2) were mixed directly in an aqueous phase while maintaining pH 1 by adding concentrated nitric acid. The acid was added to prevent formation of the agglomerates and to obtain a good dispersion of the particles. The liquid was slowly concentrated using a rotary evaporator, until the resultant suspension contained 15% TiO_2 colloid by weight. To this suspension was added ethanol equivalent to 2 times the volume of colloid and centrifuged at 5000 rpm. This washing procedure was repeated three times. The colloids were dispersed in a high-speed stirrer (15 000 rpm) by adding an ethanolic solution of ethylcellulose (10 wt %) and anhydrous α-terpineol. The final colloidal paste was prepared by evaporating of the ethanol at 50 °C under vacuum (30−50 mbar) to a final TiO_2 concentration of 20 wt % and a ratio of ethylcellulose/TiO_2 = 0.47 wt. The surface area of this mixed colloid is 75 m^2/g, and the porosity is 0.62.

The TiO_2 paste is deposited onto a sheet glass (Nippon Sheet Glass, Hyogo, Japan, which has been coated with a fluorine-doped stannic oxide layer, sheet resistance of 8−10 Ω/cm^2) using a screen printing

(19) Sheldrick, G. M. *SHELXTL PLUS*, VAX/VMS Version; Siemens Analytical X-ray Instruments Inc.: Madison, WI, 1990. Wavemetrics software.

(20) Wavemetrics: http://www.wavemetrics.com/.

(21) (a) Barbe, Ch. J.; Arendse, F.; Comte, P.; Jirousek, M.; Lenzmann, F.; Shklover, V.; Graetzel, M. *J. Am. Ceram. Soc*. **1997**, *80*, 3157. (b) Burnside, S. D.; Shklover, V.; Barbe, Ch. J.; Comte, P.; Arendse, F.; Brooks, K.; Graetzel, M. *Chem. Mater*. **1998**, *10*, 2419.

technique. The resulting layer is dried in air at 100 °C for 15 min followed by another 15 min at 150 °C. For the final processing the layers were heated using a titanium hot plate (Bioblock Scientific) to 325 °C at a rate of 30 °C/min and kept at this temperature for 5 min. Then, the temperature was raised to 375 °C at a rate of 10 °C/min and held there for 5 min. Finally the layers were fired to 450 °C at a rate of 15 °C/min under flowing oxygen and left at this temperature for 20 min before cooling to room temperature. The film thickness is 18 μm.

The heated electrodes were impregnated with a 0.05 M titanium tetrachloride solution (65 μL/cm^2) in a water-saturated desiccator for 30 min at 70 °C and washed with distilled water. (Note that the electrode contact area has to be protected from the titanium tetrachloride solution. We have used polyimide Kapton film backed by a silicone thermosetting adhesive (Dupont de Nemours).) The 0.05 M titanium tetrachloride solution was prepared in the following manner: First, 2 M titanium tetrachloride solution was prepared by adding directly titanium tetrachloride liquid into a bottle containing ice, which was cooled to −20 °C, and then the solution was further diluted to 0.05 M.

3. Synthesis

Synthesis of 4,4′,4″-Triethyl-2,2′:6′,2″-terpyridine (Et_3tpy). Freshly distilled 4-ethylpyridine (50 mL) was refluxed (170 °C) under argon with 4 g of 10% Pd on activated carbon. After 9 days, the mixture was cooled at room temperature and 500 mL of CH_2Cl_2 was added. The carbon catalyst was filtered off, washed with 100 mL of CH_2Cl_2 and the solution was reduced to dryness on rotary-evaporator. The 4-ethyl-pyridine was distilled off and then 4,4′-diethyl-2,2′-bipyridine was sublimed out of the mixture under vacuum leaving 9.5 g of 4,4′,4″-triethyl-2,2′:6′,2″-terpyridine[22] (Et_3tpy), yield 20%. The Et_3tpy ligand was used without any further purification.

^{1}H NMR (200 MHz, $CDCl_3$) δ ppm: 1.35 (6H, t, *J* 7.6 Hz, CH_3, CH_3″), 1.37 (3H, t, *J* 7.6 Hz, CH_3′), between 2.75 and 2.89 (6H, two partially overlapped quartets, *J* 7.6 Hz), 7.18 (2H, d, *J* 5.0 Hz, H5 and H5″), 8.29 (2H, s, H3′ and H3″), 8.44 (2H, s, H3′ and H5′), 8.59 (2H, d, *J* 5.0 Hz, H6 and H6″).

Synthesis of 4,4′,4″-Tricarboxy-2,2′:6′,2″-terpyridine (H_3tcterpy). Et_3tpy (9 g) was added to a stirring solution of sulfuric acid (98%, 280 mL). During the vigorous stirring, 54 g of potassium dichromate was added in small portions, keeping the temperature below 70 °C. After all of the dichromate had been added, the reaction mixture was stirred until the temperature decreased to below 40 °C. The deep green mixture was poured into 6 L of ice−water, cooled to 5 °C, and left overnight. The mixture was filtered, and the resulting solid was washed with water until the washings were colorless to yield 7.5 g of a pale yellow solid. The solid was refluxed in 190 mL of 1:1 water and 98% nitric acid for 5 h. The solution was allowed to reach room temperature and then was poured into 2 L of water/ice and kept at 5 °C overnight. The precipitate was filtered, washed with water (3 × 50 mL) and Et_2O (2 × 30 mL) and allowed to dry giving 4.3 g (36% yield) of pure 4,4′,4″-tricarboxy-2,2′:6′,2″-terpyridine (H_3tcterpy).

^{1}H NMR (200 MHz, (D_2O/NaOD) δ ppm: 7.52 (2H, d, *J* 5.0 Hz, H5 and H5″), 8.13 (2H, s, H3 and H3″), 8.31 (2H, s, H3′ and H5′), 8.43 (2H, d, *J* 5.0 Hz, H6 and H6″).

Synthesis of 4,4′,4″-Trimethoxycarbonyl-2,2′:6′,2″-terpyridine. A suspension of 4,4′,4″-tricarboxy-2,2′:6′,2″-terpyridine (1.27 g) in methanol (absolute, 150 mL) and sulfuric acid (1 mL) were refluxed for 3 days. The precipitated white crystals were filtered and washed with methanol and followed by ether. Yield 1.02 g (72%).

^{1}H NMR (200 MHz, $CDCl_3$) δ ppm: 4.05 (3H, s, CH_3′), 4.07 (6H, s, CH_3), 7.95 (2H, dd, *J* 6.0 Hz, *J* 2 Hz, H5 and H5″), 8.91 (2H, dd, *J* 6.0 Hz, *J* 1.0 Hz, H6 and H6″), 9.05 (2H, s, H3′ and H5′), 9.14 (2H, dd, *J* 2.0 Hz, *J* 1 Hz, H3 and H3″).

Synthesis of [Ru(trimethoxycarbonylterpy)Cl_3]. This complex was prepared by a modification of a published procedure.[18] Ethyl alcohol (50 mL) and ruthenium trichloride (0.26 g) were reacted under argon. After the mixture stirred for 2 min, a solution of the ligand 4,4′,4″-trimethoxycarbonyl-2,2′:6′,2″-terpyridine, 0.403 g, in 50 mL of dichloromethane, was then added. The reaction mixture was refluxed for 2 h under argon. The solution was concentrated to 20 mL, and the reaction mixture was cooled to room temperature. The precipitated complex was collected on a sintered glass crucible and was washed thoroughly with ethanol to remove unreacted ruthenium trichloride. The air-dried product was 0.485 g, yield 79%. Anal. Calcd for $C_{21}H_{17}N_3O_6Cl_3Ru$: C, 41.02; N, 6.83; H, 2.78. Found: C, 40.96; N, 6.88; H, 2.75.

Synthesis of {$(C_2H_5)_3NH$}[Ru(H_3tcterpy)$(NCS)_3$]·$2H_2O$ (1). The complex **1** was synthesized in dark under an argon atmosphere by refluxing at 130 °C, a solution of [H_4N]NCS (2 g, in 10 mL of H_2O) and Ru(trimethoxycarbonylterpy)Cl_3 complex (0.5 g, in 50 mL of DMF) for 4 h. Then, 20 mL of triethylamine and 10 mL of H_2O were added, and the solution was refluxed for a further 24 h to hydrolyze the ester groups on the terpyridine ligand. The solvent volume was reduced on a rotary evaporator to about 10 mL, and then the solution was added to 70 mL of H_2O. The resulting precipitate was filtered and dried. The isolated solid was recrystallized from methanol−diethyl ether, after which it was further purified on a 3 × 30 cm Sephadex LH-20 column, using methanol as eluent (yield 75%, 0.476 g). Anal. Calcd for $C_{27}H_{31}N_7O_8S_3$ Ru: C, 41.64; N, 12.58; H, 4.01. Found: C, 41.85; N, 12.14; H, 4.05. ^{1}H NMR (200 MHz, CD_3OD) δ ppm: 1.30 (9H, t, CH_3), 3.26 (6H, q, CH_2), 8.26 (2H, d, H5 and H5′), 8.96 (4H, s, H3, H3′, H5′ and H3″), 9.22 (2H, d, H6 and H6″).

Synthesis of {$(C_4H_9)_4N$}$_2$[Ru(H_2tcterpy)$(NCS)_3$]·$3H_2O$ (2). The complex **1** (0.476 g) was dissolved in 10 mL of water, and then the pH was increased to 9.0 by the addition of tetrabutylammonium hydroxide solution (0.05 M). The solution was filtered, and the filtrate pH was lowered to 3.5. The flask was kept in a refrigerator for 15 h, at −4 °C and was then allowed to warm to room temperature. The resulting precipitate was collected on a sintered glass crucible. Yield 69% (0.5 g). The NMR spectrum shows two tetrabutylammonium cations per ruthenium center.

Anal. Calcd for $C_{53}H_{88}N_8O_9S_3$ Ru: C, 54.01; N, 9.51; H, 7.52. Found: C, 54.66; N, 10.07; H, 7.00. ^{1}H NMR 200 MHz, (CD_3OD) δ ppm: 1.03 (24H, t, CH_3), 1.41 (16H, m, CH_2), 1.65 (16H, m, CH_2), 3.27 (16H, t, CH_2), 8.19 (2H, dd, H5 and H5″), 8.92 (4H, s, H3, H3′, H3″ and H5′), 9.13 (2H, d, H6 and H6″).

Synthesis of Complex {$(C_4H_9)_4N$}$_3$[Ru(Htcterpy)$(NCS)_3$]·$3H_2O$ (3). The complex **1** (0.4 g) was added into a flask containing 50 mL of water. To this solution was added 0.6 g of tetrabutylammonium thiocyanate, and the pH was increased to 9 by the addition of 0.1 M tetrabutylammonium hydroxide solution. The solution was filtered, and the filtrate pH was lowered to 5.0. After the solution reached a stable pH of 5.0, the flask was kept in a refrigerator for 12 h. The flask was allowed to warm to room temperature, and the resulting precipitate was collected on a sintered glass crucible. Yield 62% (0.3 g). The NMR spectrum of this compound shows the presence of three tetrabutylammonium cations per ruthenium center. The HPLC data show that the isolated complex is 98.5% pure.

Anal. Calcd for $C_{69}H_{123}N_9O_9S_3$ Ru: C, 58.36; N, 8.87; H, 8.73. Found: C, 57.89; N, 8.57; H, 8.80. ^{1}H NMR (200 MHz,

(22) Rosewear, P. E.; Sasse, W. H. F. *J. Heterocycl. Chem.* **1971**, *8*, 483.

Scheme 1

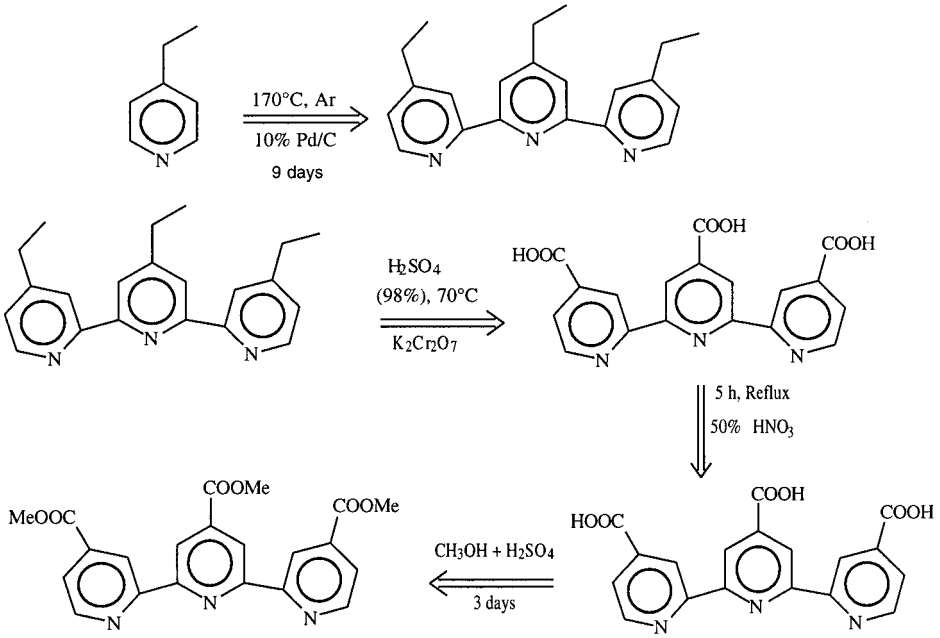

(CD_3OD) δ ppm: 1.04 (36H, t, CH_3), 1.42 (24H, m, CH_2), 1.69 (24H, m, CH_2), 3.31 (24H, t, CH_2), 8.20 (2H, dd, H5 and H5″), 8.95 (4H, s, H3, H3′, H5′ and H3″), 9.17 (2H, d, H6 and H6″).

Synthesis of $\{(C_4H_9)_4N\}_4[Ru(tcterpy)(NCS)_3]$ (4). Complex **4** was obtained by titrating complex **3** with a solution of tetrabutylammonium hydroxide. In a typical synthesis 0.1 g of complex **3** was dissolved in 10 mL of distilled water. To this solution was added dropwise 10% tetrabutylammonium hydroxide solution until the pH of the solution shows a stable reading of pH 7. At this stage, the solution was filtered through a sintered glass crucible, and the solvent was removed on a rotary evaporator at 30 °C. The resulting solid was dissolved in methanol and precipitated by the addition of 1:1 diethyl ether and petroleum ether mixture. The precipitated hygroscopic solid was dried under vacuum for 24 h.

^{1}H NMR (200 MHz, (CD_3OD) δ ppm: 1.05 (48H, t, CH_3), 1.45 (32H, m, CH_2), 1.70 (32H, m, CH_2), 3.28 (32H, t, CH_2), 8.11 (2H, dd, H5 and H5″), 8.88 (2H, d, H3 and H3″), 8.89 (2H, s, H3′ and H5′), 9.05 (2H, d, H6 and H6″).

Synthesis of $K[Ru(terpy)(NCS)_3]\cdot H_2O$ (5) (Where terpy = 2,2′:6′,2″-Terpyridine). The complex [Ru(terpy)(Cl_3)][23] (0.2 g), was reacted with an excess of potasium thiocyanate (1.1 g) ligand in DMF for 3 h. The required complex was recrystallized from methanol and a 1:1 diethyl ether and petroleum ether mixture. The complex **5** was further purified on a 3 × 30 cm Sephadex LH-20 column, using 1:1 methanol and water as an eluent.

Anal. Calcd for $C_{18}H_{13}N_6S_3OKRu$: C, 38.22; N, 14.86; H, 2.32. Found: C, 38.67; N, 14.97; H, 2.42. ^{1}H NMR (200 MHz, (CD_3OD) δ ppm: 7.68 (2H, td, H5 and H5″), 7.81 (H, t, H4′), 8.01 (2H, td, H4 and H4″), 8.32 (2H, d, H3′ and H5′), 8.36 (2H, d, H3), 9.05 (2H, d, H6 and H6″).

4. Results and Discussion

4.1. Synthetic Studies. The synthesis of 4,4′,4″-tricarboxy-2,2′:6′,2″-terpyridine in two steps involving the condensation of 4-methylpyridine followed by the oxidation with potassium dichromate has been reported.[24] However, the disadvantage of this procedure is the very low yield of 2%. The novelty of the present synthesis is the condensation of 4-ethylpyridine to produce 4,4′,4″-triethyl-2,2′:6′,2″-terpyridine, which can be oxidized to 4,4′,4″-tricarboxy-2,2′:6′,2″-terpyridine with potassium dichromate (Scheme 1). By changing the starting material from 4-methyl to 4-ethylpyridine the yield of condensed terpyridine increased 10-fold (20% yield). The lower yields of 4,4′,4″-trimethyl-2,2′:6′,2″-terpyridine are attributed to the lower reaction temperature, determined by the boiling point of the 4-methylpyridine.

The [Ru(trimethoxycarbonylterpy)(Cl_3)] complex was obtained in 79% yield by refluxing ruthenium(III) trichloride and the ligand 4,4′,4″-trimethoxycarbonyl-2,2′:6′,2″-terpyridine for 2 h under argon. The elemental analysis data of complex [Ru(trimethoxycarbonylterpy)(Cl_3)] show the presence of three chloride ligands, and the electrochemical studies indicate that the ruthenium is in 3^+ state. The reaction of complex [Ru(trimethoxycarbonylterpy)(Cl_3)] with 60-fold excess of an ambidentate thiocyanate ligand in DMF and water solution, resulted a mixture of three thiocyanate linkage isomers. The major isomer (about 60%) is the complex with three N-bonded isothiocyanates. The second isomer is tentatively assigned to N- and S-bonded isomer (approximately 20%), and the third isomer is all S-bonded (around 10%). The isomer ratios were estimated by integrating the H-6 ^{1}H NMR signals, where the three isomers show distinctly different positions. Nevertheless, in this paper we discuss exclusively the main isomer that contains all N-bonded NCS ligands.

The ruthenium metal with 4,4′,4″-tricarboxy-2,2′:6′,2″-terpyridine ligand forms a meridional configuration, in which the two peripheral pyridyl groups are *trans* to each other and electronically equivalent.[25] The central pyridine is different from the two peripheral pyridines. The ligand symmetry, which is preserved after coordination is suggestive that the pK_a of the carboxylate on the central pyridine would be different from those

(23) Sullivan, B. P.; Calvert, J. M.; Meyer, T. J. *Inorg. Chem.* **1980**, *19*, 1404.

(24) Nazeeruddin, Md. K.; Pechy, P.; Grätzel, M. Transition Metal Complex Photosensitizer and Use of This Complex in a Photovoltaic Cell. Patent, International publication number: PCT/IB 98/00680.

(25) Perez, W. J.; Lake, C. H.; See, R. F.; Toomey, L. M.; Churchill, M, R.; Takeuchi, K. J.; Radano, C. P.; Boyko, W. J.; Bessel, C. A. *J. Chem. Soc., Dalton Trans.* **1999**, 2281.

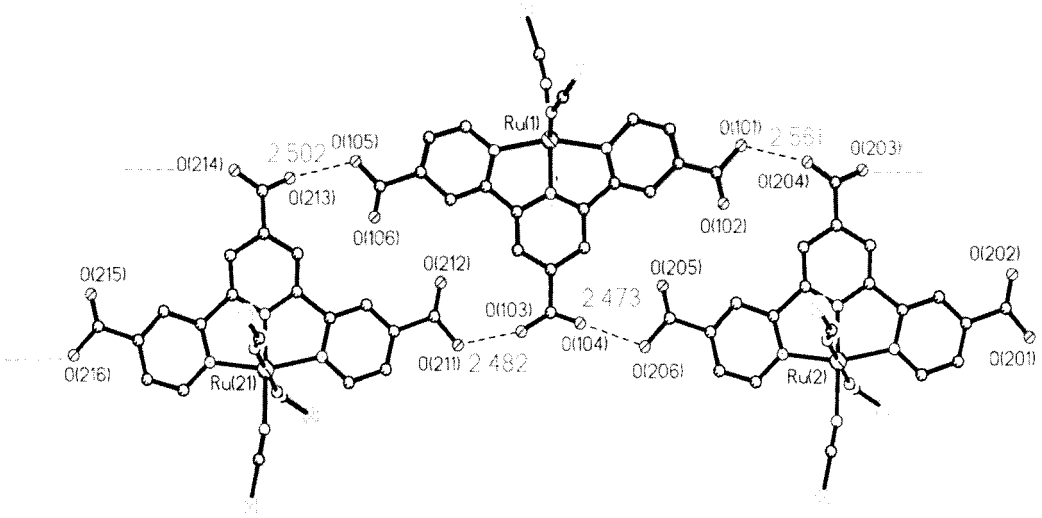

Figure 1. Strong hydrogen bonding in the crystal **2**.

Chart 1

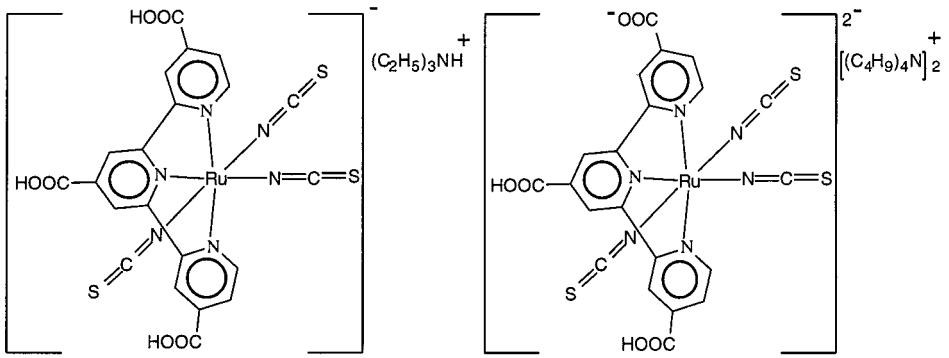

Complex **1** Complex **2**

Complex **3** Complex **4**

that are attached to the peripheral pyridines. The complex that was isolated at pH 5.0 shows the presence of only one proton that we assign to the protonation of 4′-carboxyl group of the central pyridine ring (Chart 1, complex **3**). The reason for our assignment is that the central pyridine is *trans* to the more electron-donating anionic NCS ligand compared to the two peripheral pyridine rings, which are less σ-donor compared to the NCS ligand. Hence, the π-back-bonding to the pyridine *trans* to the NCS increases the basicity of the carboxy group resulting in a higher pK_a value compared to the remaining two pyridines.[26] The theoretical calculations based on MacSpartan show that more electron density is localized on the central pyridine than on peripheral pyridines.[27] This is in agreement with our assignments for the pK_a values in complex **3**.

4.2. Crystal Structure. Small crystals of complex **2** were obtained from DMSO solution, and the structure is shown in Figure 1. The atomic coordinates together with the bond lengths and angles will be published in our subsequent paper. Complex **2** shows a "normal" geometry with a slightly distorted octahedral coordination around the Ru atoms being generated by three nitrogen donors from the terpyridine ligand and three nitrogen donors of isothiocyanate ligands.[28,29] Strong hydrogen bonds O−H···O connect molecules **2** into 2-dimensional sheets along

(26) (a) Anderson, P. A.; Anderson R. F.; Furue, M.; Junk, P. C.; Keene, F. R.; Patterson, B. T.; Yeomans, B. D. *Inorg. Chem.* **2000**, *39*, 2721. (b) Gerli, A.; Reedijk, J.; Lakin, M. T.; Spek, A. L. *Inorg. Chem.* **1995**, *34*, 1836.

(27) Wavemetrics: http://www.wavefun.com/ - Calculations were performed using MacSpartan Plus using semiempirical techniques employing PM3 parameters for the transition metal.

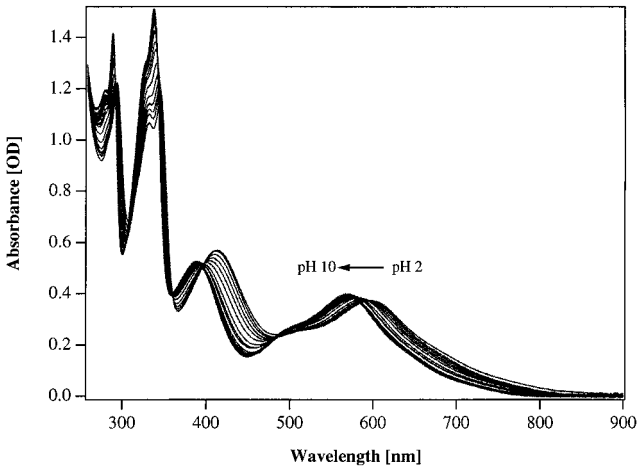

Figure 2. Absorption spectral changes of the black dye as a function of pH, measured at a concentration of 5×10^{-5} and 298 K, showing the presence of three isosbestic points.

the [111] direction of the crystal. These hydrogen bonds are very strong (O···O distances are 2.482 and 2.561 Å), indicating that the bonds are primarily due to electrostatic interactions. Strong hydrogen bonding O−H···O could also be expected in solutions of **2**, and as consequence the anchoring properties of **2** on the TiO_2 semiconductor surface will be affected. The distances between the planes are greater than 5 Å, which precludes the existence of significant π-stacking between the terpyridyl rings.

4.3. Electronic Spectra. The UV−vis, emission, and lifetime data of the black dye were measured over the pH range 2−11. The absorption spectrum of the black dye is dominated by metal-to-ligand charge-transfer transitions (MLCT). At pH 11, the black dye is the fully deprotonated anionic form and shows MLCT bands in the visible region at 570 and 390 nm, and the high energy $\pi-\pi^*$ band at 340 nm.[30] When acid is added to the black dye solution, changes in the electronic spectrum occur as shown in Figure 2. As the solution pH is lowered from 11 to 2, the MLCT transition band shifts from 570 to 600 nm with three isosbestic points at 580, 485, and 390 nm. The $\pi-\pi^*$ band shifts slightly from 340 to 345 nm. Below pH 2, precipitation under formation of a colloidal suspension of the fully protonated complex becomes apparent.

There are three carboxylic groups on the 4,4′,4″-positions of the terpyridine ligand. If the protonation is stepwise, three protonation equilibria can be envisioned corresponding to the three carboxy groups. On the other hand, if it is simultaneous, only one equilibrium constant is expected. Figure 3 shows the titration curve obtained by plotting the absorbance change at 620 and 338 nm versus pH. The plot between pH 4 to 2, shows a clear inflection point at pH = 3.3 giving the ground-state pK_a value of 3.3 ± 0.1. This we assign to concurrent dissociation of two protons coming from the peripheral pyridines. This value is similar to the ground-state pK_a's observed for ruthenium complexes of 4,4′-dicarboxy-2,2′-bipyridine ligands.[10] However, there is a second inflection point at pH = 5.0 ± 0.1, which we assign to the second ground-state pK_{a2} coming from the central pyridine that is *trans* to the NCS ligand. The solid line in Figure 3 exhibits good agreement with the experimental points, which was fitted, assuming that the complex has two pK_a values 3.3 and 5.0 at above pH 2.2.

An ethanolic solution of **1** (dark green in color, contains three protons), **2** (green in color, contains two protons), **3** (blue in color, contains one proton), and **4** (purple in color, contains no proton) shows lowest MLCT maxima at 625, 620, 610, and 590 nm, respectively (Table 2). The λ maximum of the low-energy MLCT band is red-shifted (about 5−20 nm) for each step of protonation. The 35 nm red-shift of the longer wavelength band in going from the fully deprotonated to the fully protonated tcterpy, is mainly due to the stronger electron-withdrawing nature of the COOH groups compared to the carboxylate anions at the 4,4′,4″-positions of the terpyridine ligand, which lowers the energy of π^* orbital of the ligand.[31] It is interesting to note that the extent of red-shift of the lowest MLCT band is similar in both ethanol and aqueous solution. For comparison UV−vis spectral data of an analogous unsubstituted 2,2′;6′,2″-terpyridine ruthenium complex **5**, is included in Table 2. The lowest MLCT maxima for **5** found at 570 in ethanol. The 55 nm red-shift in complex **1** compared to its unsubstituted analogue (complex **5**) is mainly due to the lower π^* orbital of the substituted terpyridine ligand.

The absorption and molar extinction coefficient data of **3** that contains the monoprotonated tctpy ligand in different polar solvents are collected in Table 3. The lowest MLCT band shifts from 570 nm (in H_2O) to 620 nm (γ-butyrolactone). It is interesting to note that there is a significant difference in the molar extinction coefficient of the complex in different organic solvents. The red-shift of 50 nm can be explained in terms of donor−acceptor interactions between the lone pair of electrons on the sulfur of the thiocyanate ligand and the solvent, causing a destabilization of the metal t_{2g} orbitals going from water to butyrolactone. The solvatochromic behavior of the black dye is consistent with the general phenomenon of the transition metal complexes that contain ligands having lone pairs of electrons.[32]

4.4. Emission Spectra. When complex **1** is excited within the MLCT absorption band at 298 K in an air-equilibrated ethanolic solution, it exhibits a luminescence maximum at 950 nm and a lifetime of 18 ± 1 ns. The emission spectral profile is independent of excitation wavelength,and the excitation spectrum matches well with the absorption spectrum. Complexes **2**, **3**, and **4** in ethanol solution show maxima at 900, 854, and 820 nm, respectively (Table 2). The difference in the λ_{max} of complex **1** from that of complex **4** is due to the low π^* orbital of tcterpy ligand in the protonated forms compared to the deprotonated form.[31] The emission intensity of complex **4** is higher than for complexes **3** and **2**.

The emission maxima of air-equilibrated aqueous solutions (contains 15% ethanol) of the black dye at pH 11 are seen at 800 nm, which red-shifts to 870 nm upon decreasing the pH to 2. No significant change in the spectral profile of the emission spectra was observed in going from pH 11 to 2. The effect of protonation on the luminescence and lifetime of the black dye is striking. The emission intensity decreases to ∼12% of the value at pH 11 (Figure 4a) and the lifetime of the MLCT excited state decreases from 22 to <3 ns, in going from pH 11 to 2 (Figure 4b). It is well established in the literature that the charge-transfer excited states can promote proton induced deactivation

(28) Shklover, V.; Bolliger, B.; Hochstrasser, M.; Erbudak, M.; Nissen, H.-U.; Zakeeruddin, S. M.; Nazeeruddin, Md. K.; Grätzel, M. *J. Solid State Chem.* **1997**, *132*, 60.
(29) Shklover, V.; Ovchinnikov, Yu. E.; Braginsky, L. S.; Zakeeruddin, S. M.; Grätzel, M. *Chem. Mater.* **1998**, *10*, 2533.
(30) Mamo, A.; Juris, A. Calogero, G.; Campagna, S. *Chem. Commun.* **1996**, 1225.
(31) Barigelletti, F.; Flamigni, L.; Guardigli, M.; Sauvage, J.-P.; Collin, J.-P.; Sour, A. *Chem. Commun.* **1996**, 1329.
(32) Indelli, M. T.; Bignozzi, C. A.; Scandola, F.; Collin, J.-P. *Inorg. Chem.* **1998**, *37*, 6084.

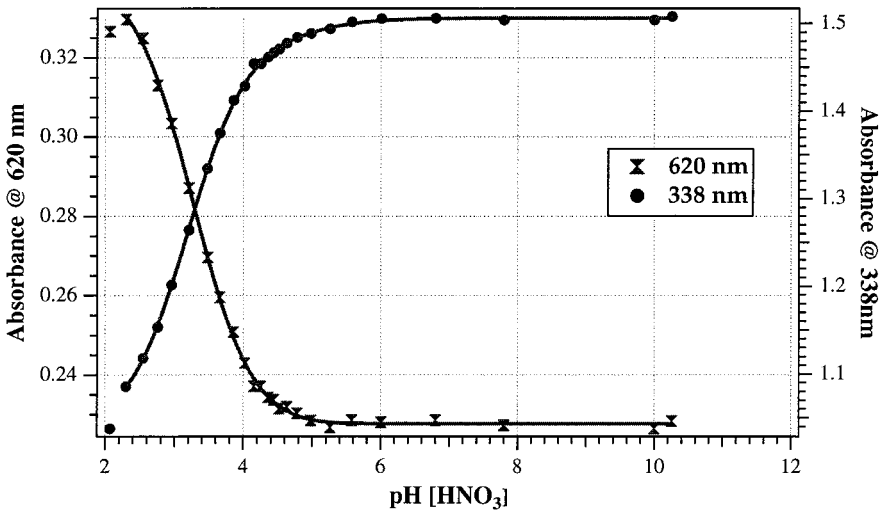

Figure 3. Absorbance change as a function of pH for the black dye at 620 and 338 nm. The solid line is calculated with the pK_a values of 3.3 and 5.0.

Table 2. Absorption, Emission, Lifetime, and Electrochemical Data of Complexes **1**−**5**

	spectroscopic data				electrochemical data[d]	
complex	abs λ_{max} (nm)[a] MLCT	$\pi-\pi^*$	em. λ_{max} (nm)[b]	τ[c] (ns)	Ru(II/III)	L/L$^-$
[Ru(H_3tcterpy)(NCS)$_3$] **1**	625, 556$_{sh}$, 429	344$_{sh}$ 330	950	18	0.72	−1.10
[Ru(H_2tcterpy)(NCS)$_3$] **2**	620, 542$_{sh}$, 413	342, 329	900	18	0.71	−1.40
[Ru(Htcterpy)(NCS)$_3$] **3**	610, 536$_{sh}$, 411	339, 328	854	30	0.66	−1.60
[Ru(tcterpy)(NCS)$_3$] **4**	590, 528$_{sh}$, 400	338, 326	820	38	0.50	−1.65
[Ru(terpy)(NCS)$_3$] **5**	570, 532, 386	318, 280	812	45	0.61	−1.50

[a] Measured in ethanol, sh = shoulder. [b] The emission spectra were obtained by exciting into the lowest MLCT band at 298 K. [c] Measured at 298 K, ± 1 ns. [d] V vs Ag/AgCl.

Table 3. Absorption and Emission Spectral Properties of Complex **3** in Different Organic Solvents at Room Temperature[a]

solvent	abs max (nm)	molar extinction coefficient ($M^{-1}cm^{-1}$)	em. max (nm)	solvent dielectric constant (ϵ)
H_2O	570	6000	829	78.4
CH_3CN	611	7320	876	36.5
C_2H_5OH	605	7480	854	24.5
CH_3OCH_2CN	610	7500	882	21.0
DMF	600	7640	815	38.2
γ-butyrolactone	620	7800	890	39.0

[a] The emission spectra were obtained by exciting at lowest MLCT band at room temperature.

and thereby shorten the excited-state lifetime and quantum yields.[33]

The emission spectral data of complex **3** recorded at ambient temperature and in different solvents (see Table 3) clearly show a strong solvent dependence. In water the emission maxima is blue-shifted compared to that in γ-butyrolactone, because of the presence of lone pair electrons on the sulfur of thiocyanate ligand that form hydrogen bonds with protonated solvents. The lifetime of **4** in methoxyacetonitrile is 71 ns, whereas in ethanol it is only 38 ns. The shorter lifetime in ethanol compared to that in the methoxyacetonitrile solvent probably is due to the hydrogen bonding that influences the excited-state lifetime of the charge-transfer excited states. On the basis of the assignments of the lowest MLCT absorption, the observed emission in complexes **1** to **4** has been assigned as originating from the Ru(tcterpy) CT excited state.[30]

The ruthenium bisterpyridine type complexes show very little emission at room temperature in solution.The excited-state lifetime of these complexes is less than a few nanoseconds due to the d−d (metal-centered) excited state becoming thermally accessible, causing deactivation of the excited state.[34] It is therefore remarkable that the complexes reported here are emitting (when compared to the ruthenium bisterpyridine complexes) at room temperature with an excited-state lifetime of 22 ns. The reason for such a long excited-state lifetime compared to the ruthenium bisterpyridine complexes could be due to the strong splitting of the t_{2g} and e_g levels of the metal orbitals caused by the thiocyanate anionic ligands. Consequently, the d−d states may not be thermally accessible at room temperature. Besides this, the electron withdrawing carboxylic acid groups located at the 4,4′,4″-positions of the tctpy ligand lower the energies of the π^*-acceptor levels of terpyridine and this also increases the gap between the ligand π^* and d−d states.[35]

Several observations can be made about the data on the emission and lifetime behavior of the black dye shown in Figure 4. The emission from the most basic form is at a higher energy and is more intense compared with that observed from the acid form. The excited-state lifetime data are consistent with the trend observed in emission intensities. The red-shifted emission from the protonated form of the complexes is due to better π-acceptor properties of the acid form and consequent lowering of the energy of the CT excited state. In other words the π orbitals of the protonated ligands are lower in energy than the deprotonated form. The energy gap law and proton-induced quenching could account for the shorter-lived emission from the acid form of the complexes: as per the "energy gap law" nonradiative decay

(33) Ayala, N. P.; Flynn, C. M., Jr.; Sacksteder, L.; Demas, J. N.; DeGraff, B. A. *J. Am. Chem. Soc.* **1990**, *112*, 3837.

(34) Hecker, C. R.; Gushurst, A. K. I.; McMillin, D. R. *Inorg. Chem.* **1991**, *30*, 538.

(35) Maestri, M.; Armaroli, N.; Balzani, V.; Constable, E. C.; Thompson, A. M. W. C. *Inorg. Chem.* **1995**, *34*, 2759.

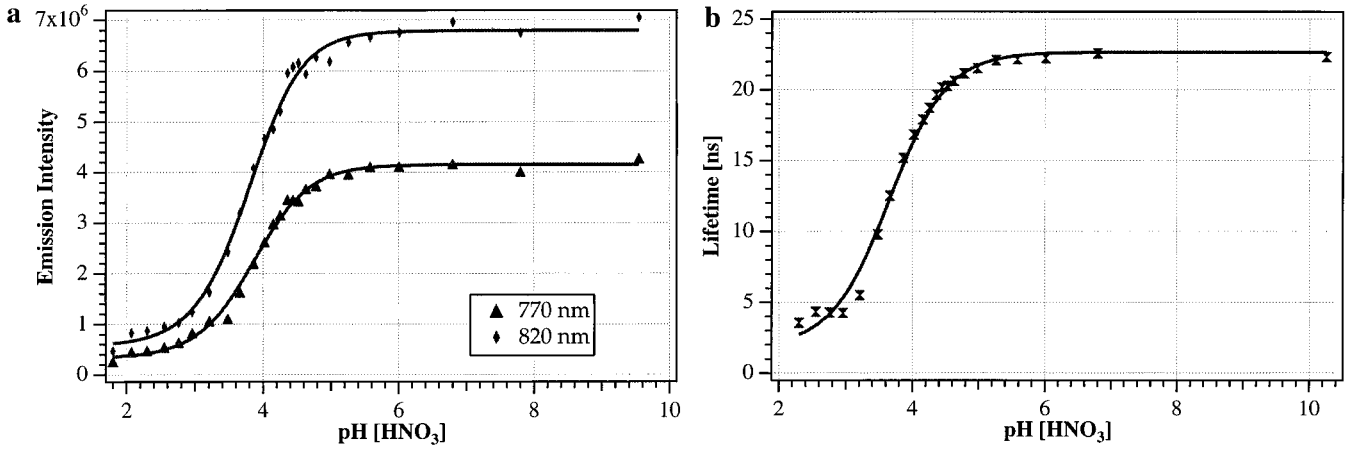

Figure 4. (a) Effect of pH on the emission intensity of the black dye at 770 and 820 nm, in air-equilibrated aqueous solution. $\lambda_{ex} = 600$ nm. (b) Excited-state lifetime of the black dye as a function of pH at room temperature in air-equilibrated aqueous solution, measured at 710 nm.

processes are expected to be more efficient in complexes with lower-energy excited states.[36]

4.5. Electrochemical Studies. The cyclic voltammogram of complex [Ru(trimethoxycarbonylterpy)Cl_3] measured in acetonitrile containing 0.1M tetrabutylammonium tetrafluoroborate shows a reversible wave at 0.38 V (vs Ag/AgCl), which is attributed to the RuIII/II redox couple.[37] The separation between the cathodic and the anodic wave is 60 mV and the peak current ratio is 0.98. The black dye containing two protons (complex **2**) shows a reversible couple at 0.71 V (vs Ag/AgCl), with a 60 mV peak separation. However, the ratio between cathodic and anodic peak current is 0.71, which decreases to 0.2 on going from a scan rate 500 to 20 mV per second. The complex **2** displays an irreversible reduction wave at −1.4 V (vs Ag/AgCl) between scan rates 500 to 20 mV per second, that we assign to the reduction of the tricarboxyterpyridine ligand. The analogous ruthenium complex **5** that contains unsubstituted terpyridyl ligand shows both reversible oxidation potential at 0.61 V and a ligand-based reduction potential at −1.5 V versus Ag/AgCl. Hence, the irreversibility of the reduction potential in complex **2** is most likely due to the presence of protons that are getting reduced on the surface of the glassy carbon electrode.[38] The 100 mV difference in the oxidation potential of complex **2** compared to complex **5** reflects the π-acceptor nature of the carboxylic groups.

Under identical experimental conditions complexes **3** and **4** show reversible wave at 0.66 and 0.5 V versus SCE, respectively. The 200 mV difference between the oxidation potentials of complex **2** and **4** is due to the presence of protons on carboxylic groups at the 4,4′,4″ positions. Complex **3** shows a quasireversible ligand-based reduction wave at −1.6 V versus Ag/AgCl. However, complex **4** shows a reversible ligand-based reduction wave at −1.65 V versus Ag/AgCl. The fact that complex **4** and the unsubstituted terpyridine complex **5** show a reversible reduction wave with 60 mV separation suggests that the irreversibility in **2** and quasi-reversibility in **3** is due to the presence of protons.

Changes in the electron-donating or electron-withdrawing nature of the ligand can result in a variation of electronic properties at the metal center. It is interesting to compare the complex [Ru(trimethoxycarbonylterpy)Cl_3] and **2** that contain chloride and thiocyanate ligands, respectively. The ruthenium metal in [Ru(trimethoxycarbonylterpy)Cl_3] is in the 3^+ state, due to the strong σ-donor nature of the halide ligands where as in complex **2**, it is in the 2^+ state. The 320 mV difference between the complex [Ru(trimethoxycarbonylterpy)Cl_3] and **2** shows the extent of π-back-bonding to the thiocyanate ligand from ruthenium(II) center.

4.6. NMR Spectroscopy Studies. The ^{1}H NMR spectrum of complex **2**, measured in CD_3OD solution shows three sharp and well resolved signals in the aromatic region, corresponding to the terpyridyl protons in which the two peripheral rings are magnetically equivalent. In a pseudo-octahedral geometry, a tridentate ligand like terpyridine coordinates to a metal center in a meridional fashion, and the thiocyanate ligands are in an orthogonal plane. The lowest-field doublet centered at δ 9.13 ppm is assigned to the H6 and H6″ proton of the pyridine ring, which is *cis* to the NCS groups. The singlet at δ 8.92 ppm is due to H3, H3′, H5′, and H3″ and the doublet centered at δ 8.19 ppm assigned to the H5 and H5″ proton.[25] However, the same complex when measured in DMSO-d_6 solvent show two singlets, at δ 9.11 and 9.08 ppm, due to the H3 and H3″ and H3′ and H5′ protons. These two singlets are downfield-shifted compared to the H6 and H6″ proton that appears as a doublet centered at δ 8.90. The H5 and H5″ proton signal shows a doublet of doublets centered at δ 8.23 ppm.

In the aliphatic region, a triplet centered at 3.27, two multiplets at 1.65, and 1.41 and a triplet at 1.03 ppm are assigned to the tetrabutylammonium cation. The integrated ratio between aliphatic protons to aromatic protons in complex **2** shows that each ruthenium center has two tetrabutylammonium cations. The complexes **3** and **4** show a similar pattern with the integral ratio between the aliphatic to aromatic protons, indicating the presence of three and four tetrabutylammonium cations per ruthenium center, respectively. However, in complex **1**, the aliphatic region show the presence of triethylammonium group and the integral ratio between the aliphatic to aromatic protons confirms the presence of one triethylammonium cation per ruthenium center.

^{13}C NMR Spectra. ^{13}C NMR spectra of complex **3** show 12 resonances corresponding to the coordinated 4,4′,4″-tricarboxy-2,2′:6′,2″-terpyridine ligand (Figure 5). The two downfield resonances at 168.57 and 168.23 are assigned to the carboxylate carbons of the peripheral (C7) and the central (C7′) pyridines, respectively. The two peaks at 162.21 and 160.74 are assigned to C2′ and C2 carbons, which are near to the electron-withdrawing nitrogen of the coordinated pyridine. The more

(36) Kalyanasundaram, K.; Nazeeruddin, Md. K. *Inorg. Chem.* **1990**, *29*, 1888.
(37) (a) Liobet, A.; Doppelt, P.; Meyer, T. J. *Inorg. Chem.* **1988**, *27*, 514. (b) Samuels, G. J.; Meyer, T. J. *J. Am. Chem. Soc.* **1981**, *103*, 307.
(38) Bond, A. M.; Deacon, G. B.; Howitt, J.; MacFarlane, D. R.; Spiccia, L.; Wolfbauer, G. *J. Electrochem. Soc.* **1999**, *146*, 648.

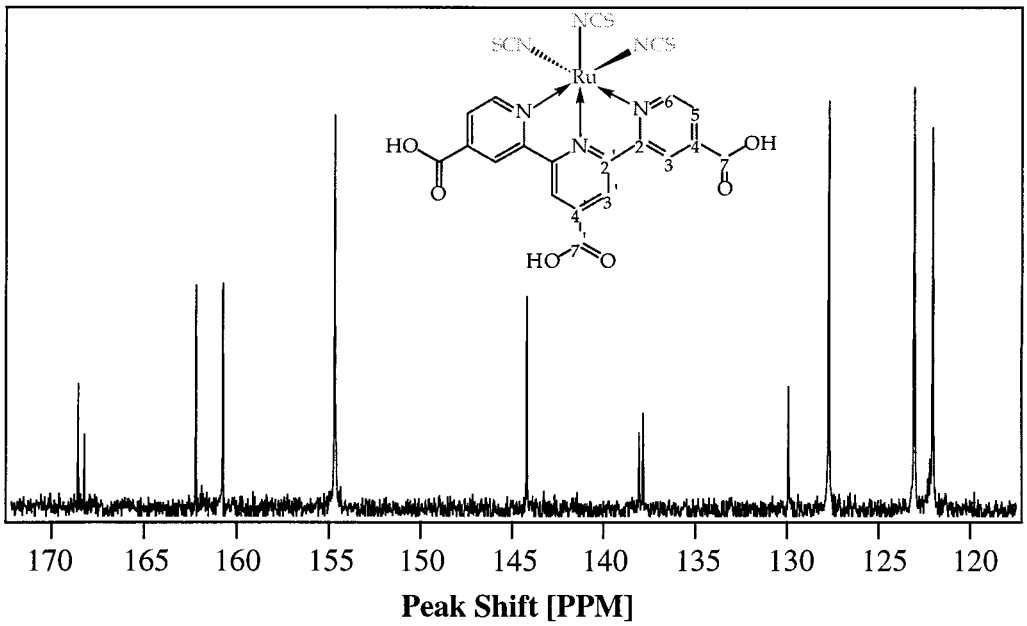

Figure 5. ^{13}C NMR specrum of $\{(C_4H_9)_4N\}_3[Ru(Htcterpy)(NCS)_3]$ complex in CD_3OD at room temperature.

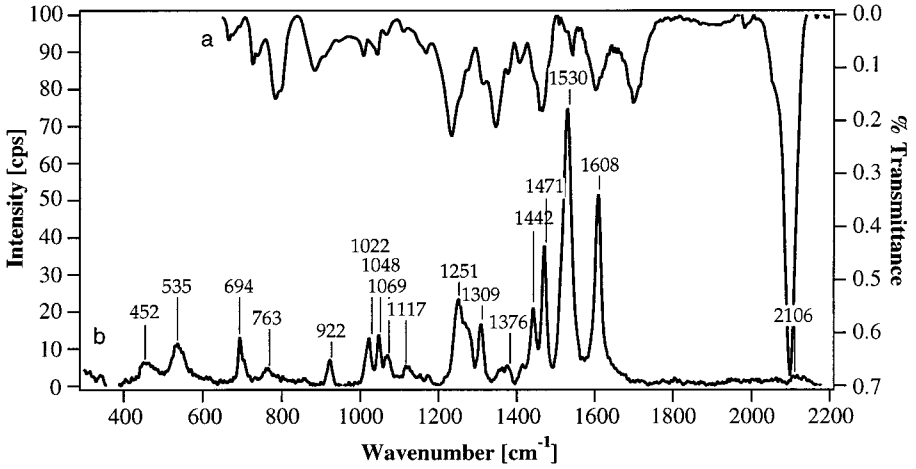

Figure 6. Infrared (a) and Raman (b) spectra of $\{(C_4H_9)_4N\}_3[Ru(Htcterpy)(NCS)_3]$.

intense peak at 154.68 ppm is due to C6 carbon. The C3′, C3, and C5 carbons were observed at 127.72, 123.06 and 122.05 ppm, respectively. The peaks at 138.06 and 137.843 are due to quaternary C4′ and C4 carbons and the intensities of these carbons are significantly lower than the C3, C5, and C6 carbons.[25]

The peaks at 129.93 and 144.19 ppm are assigned to the NCS that is in the plane of the tctpy ligand and the *trans* NCS ligands, respectively. It is striking to note the difference in the peak position between the two types of NCS carbons. The carbons of the mutually *trans* NCS ligands are more deshielded (144.19 ppm) compared to the NCS ligand that is *trans* to the cental pyridine nitrogen in tctpy (129.93 ppm). The most likely reason for such an unusual shift could be that in the axial position both thiocyanate ligands are having less π-back-bonding compared to *cis* NCS. Our assignments for the NCS ligands are based on the known ruthenium complexes that contain *cis* and *trans* NCS ligands.[39] Finally, there are four resonance peaks in the aliphatic region, at δ 59.62, 24.85, 20.77, and 14.04 ppm due to the tetrabutylammonium group (not shown in Figure 5).

4.7. Infrared and Resonance Raman Spectroscopic Studies. The IR and RR spectra of complex **3** in the region 400−2200 cm^{-1} are shown in Figure 6. The complex **3** shows a strong and intense absorption at 2106 cm^{-1} that we assign to the N-coordinated υ(CN). This band is approximately 4 times more intense than the band at 788 cm^{-1}, due to υ(CS). The bands at 1713 and 1603 cm^{-1} are assigned to the C═O stretching bands of protonated and deprotonated carboxy groups of complex **3**, respectively. It is interesting to compare the ratio between the protonated and deprotonated carbonyl (C═O) stretch of these complexes. Complex **3**, which contains one protonated and two deprotonated carboxy groups, shows a ratio of about 1:1. In contrast, complex **2**, which contains two protonated and one deprotonated carboxy groups, shows a ratio of 3:1. Complex **4** shows a single band at 1600 cm^{-1} due to carboxylate C═O stretch. The ring-stretching modes for $[Ru(bpy)_3]^{2+}$ were reported at 1608, 1563, 1491, and 1450 cm^{-1}.[40] The three bands at 1542, 1463, 1410 cm^{-1} in complex **3** are assigned to the ring-stretching modes of tcterpy ligand, and the apparent differences are due to the substitution effect on the terpyridine ligand. The three peaks between 2870 and 2970 are (not shown in Figure 6) assigned to the tetrabutylammonium symmetric and asymmetric υ(C−H) modes.[41]

(39) Zakeeruddin, S. M.; Nazeeruddin, Md. K.; Humphry-Baker, R.; Grätzel, M. *Inorg. Chim. Acta* **1999**, *296*, 250.

(40) Strommen, D. P.; Mallick, P. K.; Danzer, G. D.; Lumpkin, R. S.; Kincaid, J. R. *J. Phys. Chem.* **1990**, *94*, 1357.

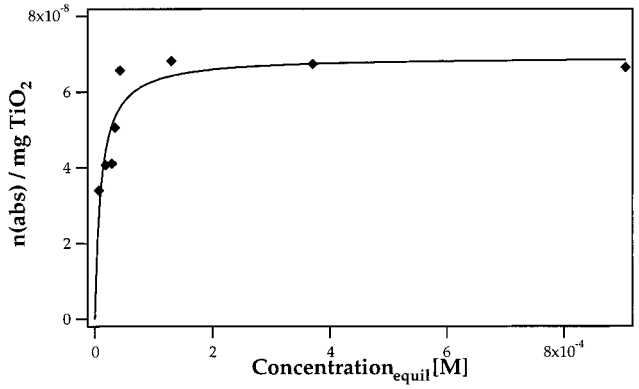

Figure 7. Amount of dye adsorbed as a function of the equilibrium concentration in the solution.

RR spectroscopy was used to confirm the ligand responsible for the localization of the electron density upon excitation. Excitation into an MLCT gives rise to resonance enhancements of the symmetric stretching A_1 modes of that ligand. For a broad visible absorption spectrum as seen in complex **3**, several overlapping MLCT transitions are possible. The relative contribution of each transition can be ascertained by examining the resonance enhancement of the vibrational modes for the different ligands as a function of the probing Raman wavelength. Other groups have demonstrated the utility of this method to map out the MLCT chromophores.[42]

By selecting a wavelength at 568.2 nm, in aqueous **3** solution, RR shows a spectrum whose fingerprint in terms of peak position is analogous to the 2,2′;6′,2″-terpyridine ligand. Besides the C−H stretch modes from 2800 to 3050 cm^{-1}, the region that is most useful for the characterization of the ligand is from 1000 to 1700 cm^{-1}. By analogy with the enhanced modes for the corresponding $Ru(tcterpy)_2$ complexes, the tcterpy ligand is seen to exhibit bands at 1608, 1530, 1471, 1442, 1309, 1278, 1251, 1048, 1022 cm^{-1}. For complex **3**, excitation at 520.8 and 468.0 nm gives rise to the same pattern of frequencies. These peaks are derived from the pyridine ring stretch and deformation modes. This suggests that the visible part of the absorption spectrum of the black dye is dominated by transitions of MLCT nature, with migration of charge from the Ru orbitals to the low π^* orbitals on the tcterpy ligand. At shorter wavelengths, higher-energy π^* electronic states are probed in accordance with calculations but no large change in resonance enhancement is observed.

4.8. Langmuir Isotherm for Adsorption of Complex 3 at the Surface of TiO_2. Adsorption studies were carried out on transparent TiO_2 films of a known thickness. The dye solution was prepared in methoxyacetonitrile. The amount of dye adsorbed as a function of the equilibrium concentration in the solution is depicted in Figure 7. The fitted line is calculated from the following equation of a Langmuir isotherm.

$$n_{ads} = K_{ads} n_\infty C_{equil}/(1 + K_a C_{equil})$$

The obtained adsorption equilibrium constant K_{ads} is $(1.0 \pm 0.3) \times 10^5$ M^{-1}, and the amount of dye adsorbed at saturation is n_α $(6.9 \pm 0.3) \times 10^{-8}$ mol/mg of TiO_2. The specific surface area obtained from BET experiments for transparent films is 100 m^2/g of TiO_2. From the value of n_α, a surface concentration of 6.9×10^{-7} mol/m^2 is estimated. Assuming full coverage of the TiO_2 surface, this corresponds to an area of 2.4 nm^2 per complex **3**. The effective surface area of this molecule is approximately 1.6 nm^2 indicates that n_∞ does not correspond to a full coverage of the TiO_2 surface by the complex **3**.

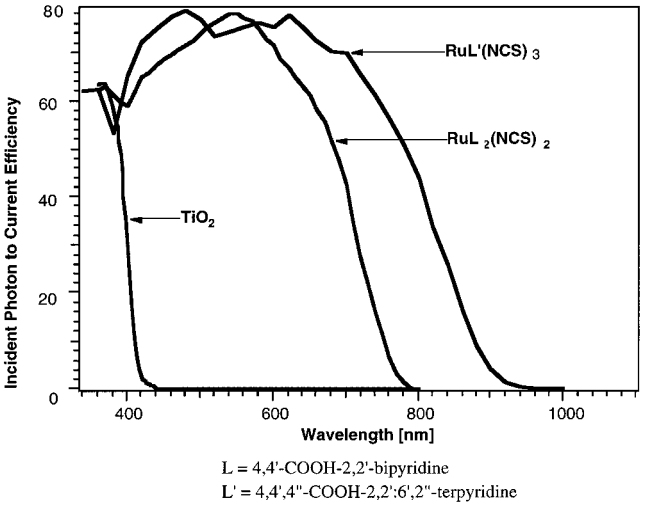

L = 4,4'-COOH-2,2'-bipyridine
L' = 4,4',4"-COOH-2,2':6',2"-terpyridine

Figure 8. Photocurrent action spectrum obtained with the black dye (complex **3**) attached to nanocrystalline TiO_2 films. The incident photon to current conversion efficiency is plotted as a function of the wavelength of the exciting light. Photocurrent action spectra for bare TiO_2 and TiO_2 doped with N3 have been included for comparison.

Under similar conditions the N3 dye shows a surface concentration of $(1.05 \pm 0.06) \times 10^{-7}$ mol/m^2.[43] The size of the N3 dye is very similar to complex **3**. The possible explanation for such an astonishing difference in n_α between the N3 dye and the complex **3**, could be the charge of the complexes. The N3 dye is a neutral molecule, whereas the complex **3** is anionic. Hence, the adsorbed species (complex **3**) are expected to show lateral Coulombic repulsion. Besides the Coulombic repulsion, the orientation of adsorbed sensitizer on the surface may also be responsible for lower surface concentration of the dye. The other possible explanation is that the dye solution of complex **3** still may contain hydrogen-bonded linear oligomers that prevent penetrating into the small pores of the TiO_2 surface. We are at present optimizing the dye uptake process, and if the dye uptake is comparable to the N3 dye, then one could expect to obtain in essence higher current densities using the complex **3**.

4.9. Photovoltaic Measurements. The dye solutions were prepared in ethanol (2×10^{-4} M) and to which was added 20 mM of taurochenodeoxycholic acid sodium salt. The TiO_2 electrodes, which were treated with titanium tetrachloride solution were heated to 500 °C at a rate of 35 °C/min under oxygen and left at this temperature for 10 min and then allowed to cool to ∼100 °C. The hot electrodes were immersed into the dye solution for 20 h. The black-colored films exhibited striking performance when tested in a photovoltaic cell in conjunction with a redox electrolyte. The composition of the electrolyte is 0.6 M dimethylpropylimidazolium iodide, 0.1M of iodine, 0.5 M *tert*-butylpyridine, and 0.1 M of lithium iodide in methoxyacetonitrile.

Figure 8 shows the photocurrent action spectrum of such a cell containing complex **3**, where the incident photon to current conversion efficiency is plotted as a function of wavelength. The broad feature appears covering the entire visible spectrum and extending into the near-IR region up to 920 nm, the incident

(41) Finnie, K. S.; Bartlett. J. R.; Woollfrey. J. L. *Langmuir* **1998**, *14*, 2744.

(42) Yabe, T.; Orman, L. K.; Anderson, D. R.; Yu, S.-C.; Xu, X.; Hopkins, J. B. *J. Phys. Chem.* **1990**, *94*, 7128.

(43) (a) Fillinger, A.; Parkinson, B. A. *J. Electrochem. Soc.* **1999**, *146*, 4559. (b) Nazeeruddin, Md. K.; Cevey, L.; Grätzel, M. Unpublished results.

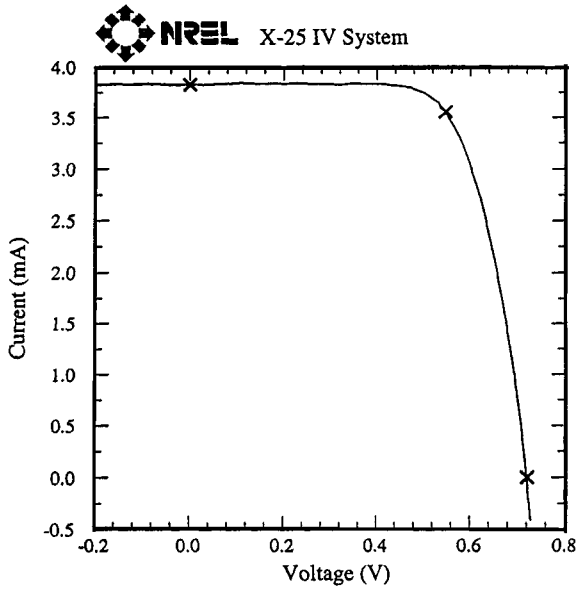

Figure 9. Photocurrent−voltage characteristics of a nanocrystalline photoelectrochemical cell sensitized with the complex **3**. The results were obtained at the NREL calibration laboratory measured at 25 °C with an area of 0.1863 cm^2 and irradiance of 1000 W m^{-2}. $V_{oc} = 0.72$ V, $I_{max} = 3.55$ mA, $J_{sc} = 20.53$ mA cm^{-2}, fill factor = 70.41%, $V_{max} = 0.546$, $I_{sc} = 3.82$ mA, $P_{max} = 1.94$ mW, and the efficiency = 10.4. The fully drawn line represents the experimentally recorded current and voltage curve. The three crosses indicate (from left to right): the short circuit current, the location of the maximum power point, and the open circuit voltage.

photon-to-current conversion efficiency (IPCE) value in the plateau region being about 80%. Taking into account the light losses in the conducting glass due to optical interfaces, the efficiency of electric current generation is practically 95% over a broad wavelength range extending from 400 to 700 nm. The overlap integral of this curve with the standard global AM 1.5 solar emission spectrum yields a short circuit photocurrent density (isc) of 20 mA/cm^2. The open circuit potential (Voc) is 720 mV, and the fill factor (ff) is 0.7, yielding for the overall solar (global AM 1.5 solar irradiance 1000 W m^{-2}) to chemical conversion efficiency a value of 10.4%. These results were confirmed at the National Renewable Energy Laboratory (NREL), Golden, Colorado, U.S.A. The measurements reported in Figure 9 were performed with a cell endowed with a antireflective coating. For normal conducting glass, the photocurrent is expected to be about 4% lower. Routinely, the photocurrents obtained with the black dye are in the range of 18−21 mA/cm^2 using the 18 μ thick nanocrystalline TiO_2 layers prepared as described in the Experimental Section. Under similar conditions the N3 dye produces about 3 mA/cm^2 lower photocurrents, the open circuit being in the 0.68−0.72 V range for both sensitizers. The fill factor depends to a large degree on current collection geometry and the viscosity of the electrolyte employed. Values exceeding 0.7 have been obtained with both dyes. Thus, there can be no question that the overall photovoltaic performance of the black dye supersedes that of the N3 sensitizer due to its superior panchromatic light-harvesting properties combined with nearly quantitative electron injection from the excited dye into the conduction band of the nanocrystalline TiO_2 film.

In contrast, complex **2** under similar conditions, shows an IPCE value of 50% in the plateau region and the open circuit voltage of 670 mV, with a fill factor of 0.65. On the other hand complex **4** shows 70% efficiency and the open circuit voltage of 750 mV, with a fill factor of 0.68. These data indicate that the performance characteristics of the complex **3** is superior to **2** and **4**. The low IPCE value of complex **2** is attributed to the formation of hydrogen-bonded aggregates on the surface. The higher open circuit potential of complex **4** is due to the absence of protons. Therefore, the photovoltaic performance of complex **3** carrying one proton is superior to complexes **2** and **4** containing two and no protons, respectively. On the basis of our findings, it is apparent that the number of protons carried by the sensitizer plays a significant role in IPCE values. Our results on the effect of protonation are consistent with the N3 data, where we found that the complex containing two protons is superior to that with four and no protons.[10b]

5. Conclusions and Perspectives

We have succeeded in developing a panchromatic sensitizer based on ruthenium complexes having carboxylated terpyridyl and three thiocyanate groups as ligands. The absorption and emission maxima of the black dye show a bathochromic shift with decreasing pH and exhibit pH-dependent excited-state lifetimes. Langmuir isotherm for adsorption of complex **3** at the surface of TiO_2 films show a surface concentration of 6.9 $\times$ 10^{-7} mol/m^2, which is 30% lower than the full monolayer coverage. On the basis of photovoltaic performance measured under full AM 1.5 sunlight, this black dye is superior to all charge-transfer sensitizers known thus far. The spectral response in the red and near-IR region is enhanced with respect to the widely used N3 dye, resulting in higher short circuit photocurrents, even though its surface coverage and its extinction coefficient are significantly lower that the values for the latter dye. At present the certified short circuit current under standard AM 1.5 sun light is 20.5 mA/cm^2, and the open circuit voltage is 0.72 V, yielding an overall conversion efficiency of 10.4 %. The discovery that the black dye exhibiting enhanced light-harvesting in the red and near-IR region opens up the way to improve significantly the overall efficiency of nanocrystalline photovoltaic devices. Thus, this class of compounds provides the basis for the design of new compounds containing anchoring phenyl and diphenyl substituents on the 4,4′,4″-positions of 2,2′;6′,2″-terpyridine. The phenyl substitution should increase the molar extinction coefficient, permitting a reduction in film thickness which should benefit the open circuit potential and overall efficiency of these solar cells.

Acknowledgment. We acknowledge financial support of this work by the Swiss National Science Foundation, the Swiss Federal Office for Energy (OFEN), and the Institute for Applied Photovoltaics (INAP, Gelsenkirchen, Germany). We thank Drs. G. Rothenberger, N. Vlachopoulos, F. P. Rotzinger, and K. Kalyanasundaram for their valuable discussions and M. Jirousek for her excellent assistance with the laboratory work. We are indebted to Dr. M. Wörle (Laboratory of Inorganic Chemistry, Swiss Federal Institute of Technology, Zürich) for the assistance in the recording of experimental X-ray data.

JA003299U